

Supporting Information

Trace Cs Induced Phase Transition of Mn₂O₃ for Enhanced Magnesium Ion Capacitors

Mudi Li,^a Yaxi Ding,^a Siwen Zhang,^{*a} Minghui Liu,^a Ying Sun,^a Yusheng Zhang,^c Bosi Yin,^{*a} Tianyi Ma^{*b}

^a Institute of Clean Energy Chemistry, Key Laboratory for Green Synthesis and Preparative Chemistry of Advanced Material, College of Chemistry, Liaoning University, Shenyang 110036, P. R. China

^b School of Science, RMIT University, Melbourne VIC 3000, Australia

^c School of Chemistry and Chemical Engineering, Hunan University of Science and Technology, Xiangtan 411201, China

*** Corresponding authors.**

E-mail address: tianyi.ma@rmit.edu.au (T. Y. Ma), zhangsiwen@lnu.edu.cn (S. W. Zhang), yinbosi@lnu.edu.cn (B. S. Yin)

Experimental Section

1. Sample preparation

Synthesis of Mn₂O₃ and CMO

0.5 g C₆H₈O₇ and 1 g Mn(CH₃COO)₂ are put into the deionized water (DI) (100 mL). And then, stir the above solution with a glass rod to obtain a clear and colorless solution. Subsequently, add 5 M NaOH dropwise until the solution turns dark orange. Next, the above solution is transferred to the Teflon-lined sealed autoclave in order to conduct hydrothermal reaction, and set the temperature to 150 °C and time to 3 h. Then, centrifuge washing of the reacted solution with ethanol and DI three times. Put the product in a vacuum drying oven and dry at 60 °C for 12 h. Finally, transfer the dried powder to a muffle furnace and calcine at 500 °C for 1 h under the condition of 2 °C min⁻¹ and the Mn₂O₃ can be obtained. As for the CMO, the only difference is that 0.1 g of CsCH₃COO is added together with the 0.5 g C₆H₈O₇ and 1 g Mn(CH₃COO)₂ in the initial hydrothermal process.

2. Electrochemical measurements

The electrochemical performances test of the electrodes and aqueous magnesium ion capacitors are carried out by NEWARE battery test system, multi-channel electrochemical analyzer (VMP3, Bio-Logic-Science Instruments) and CHI (760E, Chenhua) under the room temperature, including constant current charging and discharging (GCD) and galvanostatic intermittent titration technique (GITT) (The titration time of the charging process is 600.05 s, the titration time of the discharging process is also 600.05 s and the rest time is 600 s), cyclic voltammetry (CV), as well as

Electrochemical Impedance Spectroscopy (EIS) electrochemical workstation which is tested under the open circuit potential from 10 mHz to 600 kHz.

3. Details of assembling a three-electrode cell system

The cathode materials of Mn_2O_3 and CMO are tested in the three-electrode cell system with Hg/HgO as the reference electrode and graphite rods as the counter electrodes in the 0.5 M MgSO_4 . The preparation of working electrodes mainly involves taking the Mn_2O_3 or CMO, Super P and Polyvinylidene fluoride (PVDF) in a ratio of 8:1:1 in the N-methylpyrrolidone (NMP) solution, making viscous slurry adhere on the surface of hydrophilic carbon paper, as well as putting it into the vacuum drying oven for 12 hours at 60 °C. The loading amount of active material on each electrode which is approximately 1.5 mg and the electrode area of Mn_2O_3 and CMO in three-electrode cell are all 1.13 cm^2 .

4. Details of assembling the $\text{Mn}_2\text{O}_3/\text//\text{AC}$ and $\text{CMO}/\text//\text{AC}$

The preparation of the cathode electrode is consistent with the situation of the three-electrode cell system. As for the anode electrode, activated carbon (AC), Super P and PVDF are mixed in a ratio of 8:1:1 in the N-methylpyrrolidone (NMP) solution until they become a viscous slurry which will be coated on carbon paper dried in a vacuum drying oven for 12 h at 60 °C. CR2032 type coin cells are assembled with the Mn_2O_3 electrode or CMO electrode (The loading amount of active material on each electrode which is approximately 1.5 mg and the electrode area of Mn_2O_3 and CMO in full cell tests are all 1.13 cm^2), AC electrode and 0.5 M MgSO_4 electrolyte by the traditional methods. In order to fully utilize the capacity potential of various electrodes,

the load mass of anode electrode, AC, is calculated based on the following four equations[1]:

$$C_{sp} = \frac{It}{m\Delta U} \quad (1)$$

$$Q_- = Q_+ \quad (2)$$

$$Q = C_{sp} \times \Delta U \times M \quad (3)$$

$$\frac{M_-}{M_+} = \frac{(C_{sp,+}) \times (\Delta U_+)}{(C_{sp,-}) \times (\Delta U_-)} \quad (4)$$

Where C_{sp} represents specific capacitance, I represents the constant discharge current, t represents the discharge time, m represents the mass loading, ΔU represents potential window and M represents the mass loading of the working electrode.

Furthermore, the energy density (E) and power density (P) of the capacitors are calculated by equations as following:[2]

$$E = \frac{1}{2} C_{sp} V^2 \quad (5)$$

$$P = \frac{E}{t} \quad (6)$$

Where C_{sp} represents specific capacitance, V represents the voltage window of the cell and t represents the discharge time.

5. Material Characterizations

The phases purity of Mn_2O_3 and CMO are identified by XRD using a Rigaku Smartlab SE with Cu K α radiation ($\lambda = 0.15418$ nm). The chemical compounds of two samples are identified by XPS (Thermo Scientific K-Alpha) and the data is calibrated

by referencing the C 1s peak value to 284.8 eV. The specific surface area and porosity analysis of two samples are identified by BET (Micromeritics Tristar II 3020). The chemical structures of two samples are identified by FTIR (Thermo Scientific Nicolet iS20). The morphologies of two samples are observed by SEM (HITACHI, SU8010) and TEM (JEM-2100).

Table S1. The comparison of the peak area of Cs 3d Mn 2p, and O 1s of CMO

XPS	peak area	peak area
Cs 3d	1987.02 (Cs 3d _{3/2})	3093.14 (Cs 3d _{5/2})
Mn 2p	11460.45 (Mn 2p _{1/2})	22622.75 (Mn 2p _{3/2})
O 1s	20819.856	\

Table S2. The comparison of capacity between this work and other previously reported literatures in the three-electrode cell system.

Electrode Materials	Electrolyte	Current density (A/g)	Capacity (mAh/g)	Ref.
CMO	0.5 M MgSO ₄	0.1	214.442	This work
Al _x MnO _{2-z}	0.5 M MgSO ₄	0.1	197.02	[1]
Ni _{0.3} -Mg-1	0.5 M MgSO ₄	0.01	195.4	[2]
FeVO ₄ /C	1 M MgSO ₄	0.05	184.2	[3]
Mg-OMS-1/graphene	0.5 M Mg(NO ₃) ₂	0.02	194.1	[4]
1.6-Mg-OMS-7	0.5 M MgSO ₄	0.01	150.8	[5]
Mg-OMS-1	0.2 M MgCl ₂	0.1	115	[6]
Mg-OMS-2/graphene	0.5 M MgCl ₂	0.1	117	[7]
Mg-OMS-1	0.2 M Mg(NO ₃) ₂	0.1	103	[8]
Prussian blue type nickel hexacyanoferrate (PBN)	1 M MgSO ₄	0.1	65	[9]
LVP	4 M Mg(TFSI) ₂	0.1	102.104	[10]
Mn ₃ O ₄ -M	2 M MgSO ₄	0.1	105.8	[11]
Mn ₃ O ₄ -A	1 M MgSO ₄	0.2	98.9	[12]
Mg ₂ MnO ₄	1 M MgSO ₄ +0.1 M MnSO ₄	0.16	116.1	[13]
Na _{0.7} MnO _{2.05}	1 M MgSO ₄	0.1	22	[14]
Li ₃ V ₂ (PO ₄) ₃	0.5 M Mg(ClO ₄) ₂ /PC	0.5	85	[15]
FeVO ₄ ·0.9H ₂ O/Graphene	1 M MgSO ₄	0.5	86.6	[16]
MO-2/MWCNT	0.5 M MgSO ₄	1	56.8	[17]
MgFe _{1.33} Mn _{0.67} O ₄ (MFM-2)	0.5 M MgCl ₂	1	78.5	[18]
δ-MnO ₂ @MWCNTs/CC	0.5 M MgSO ₄	1	64.8	[19]
V ₂ O ₅	0.8 M Mg(TFSI) ₂ -85%PEG-15%H ₂ O	1	54	[20]

Table S3. The comparison of energy density between this work and other aqueous energy storage devices.

Cathode//Anode	Electrolyte	Voltage (V)	Energy density (Wh/kg)	Ref.
CMO//AC	0.5 M MgSO ₄	1.9	124.91	This work
ECMB//polyimide	0.5 M Mg(ClO ₄) ₂	2.2	65.2	[21]
δ -MnO ₂ @MWCNTs/CC//AC	0.5 M MgSO ₄	2	63.3	[19]
Mg ₂ MnO ₄ //PI	1 M MgSO ₄ +0.1 M MnSO ₄	1.6	60.1	[13]
NiCo-120// AC	2 M KOH	1.6	50.5	[22]
AMO//AC	0.5 M MgSO ₄	1.9	104.86	[1]
Mg-OMS-1//FeVO ₄ ·0.9H ₂ O/Graphene	1 M MgSO ₄	1.8	58.5	[16]
MnNiCo ₂ O ₄ NHB//YP-50	2 M Na ₂ SO ₄	2	45.4	[23]
MnO ₂ /CNTs//NaTi ₂ (PO ₄) ₃	1 M Na ₂ SO ₄ -2 M MgSO ₄	1.8	46.5	[24]
Mg-OMS-2/Graphene//AC	0.5 M Mg(NO ₃) ₂	2	46.9	[7]
PBN//Polyimide	1 M MgSO ₄	1.55	33	[9]
Ni/SnS ₂ @Ni(OH) ₂ -CC//AC	1 M KOH+20 mM ZnO	1.6	35.3	[25]
Mn-Ni LDO-C//AC	1 M KOH	2	39.1	[26]
NaMnO ₂ //NaTi ₂ (PO ₄) ₃	2 M CH ₃ COONa	1.8	30	[27]
Mn ₃ O ₄ -M//AC	2 M MgSO ₄	2	20.2	[11]
Ni-Zn-Fe-LDH//AC	6 M KOH	1.17	14.9	[28]
Mo-NiS ₂ @NiCo-LDH//AC	6 M KOH	1.6	20.3	[29]
Nb ₂ O ₅ //AC	0.5M ZnSO ₄	2	60	[30]

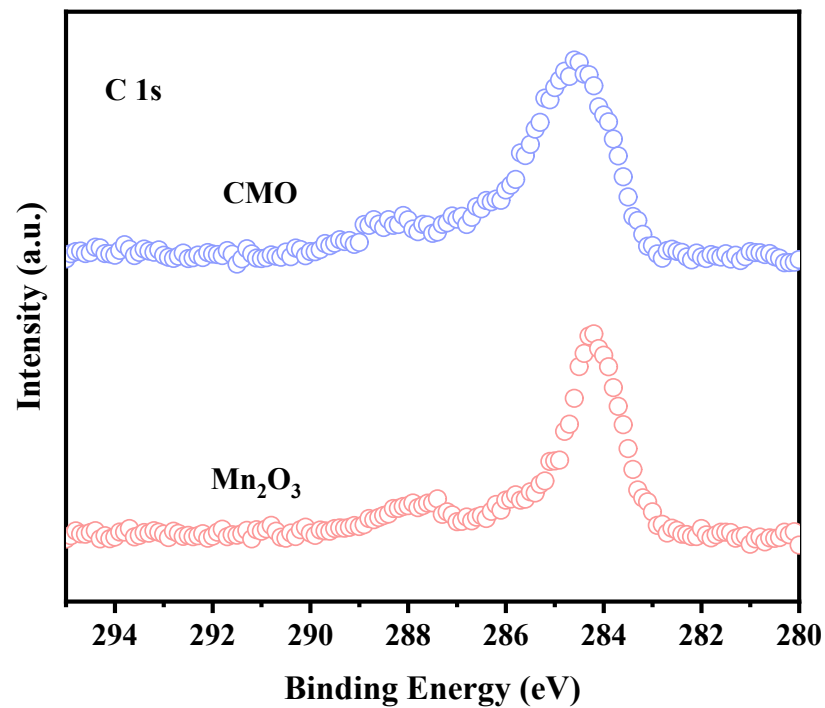


Fig. S1. The C 1s spectra of Mn_2O_3 and CMO

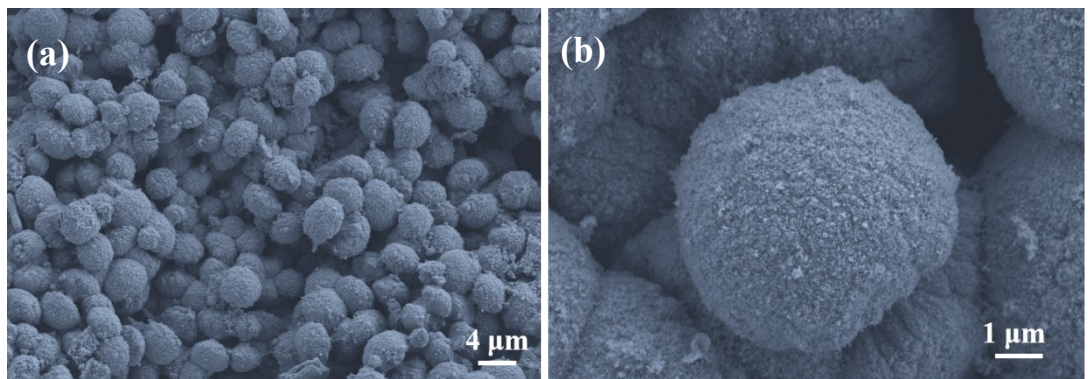


Fig. S2. (a-b) SEM image of the Mn₂O₃.

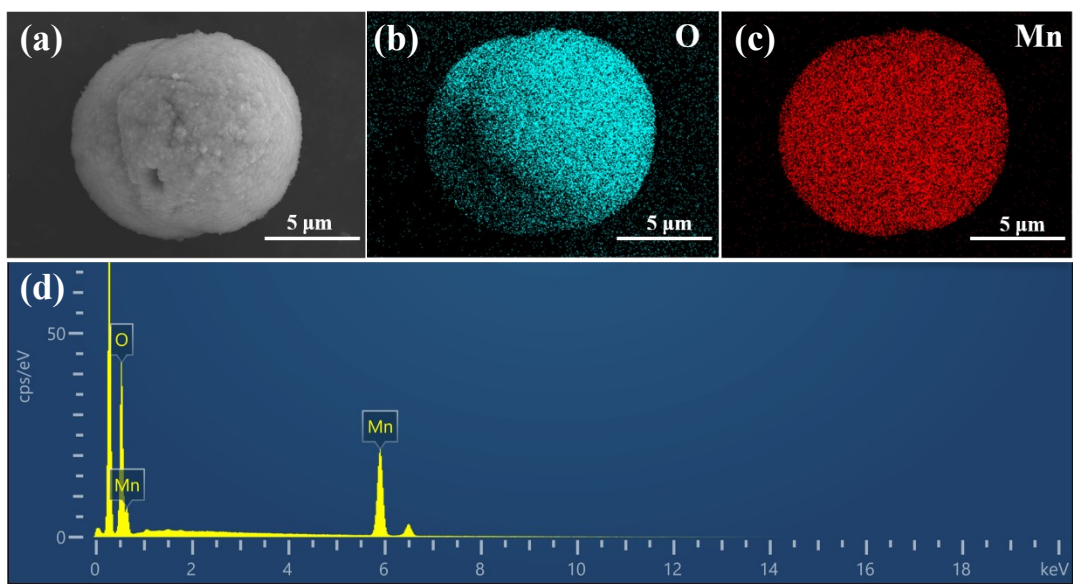


Fig. S3. (a-d) The elemental mapping images and EDS images of the Mn_2O_3 .

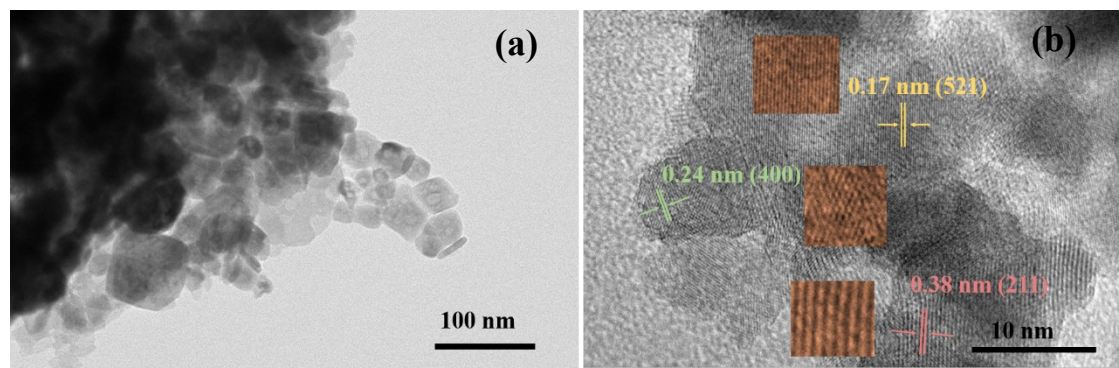


Fig. S4. (a-b) TEM image of the Mn_2O_3 .

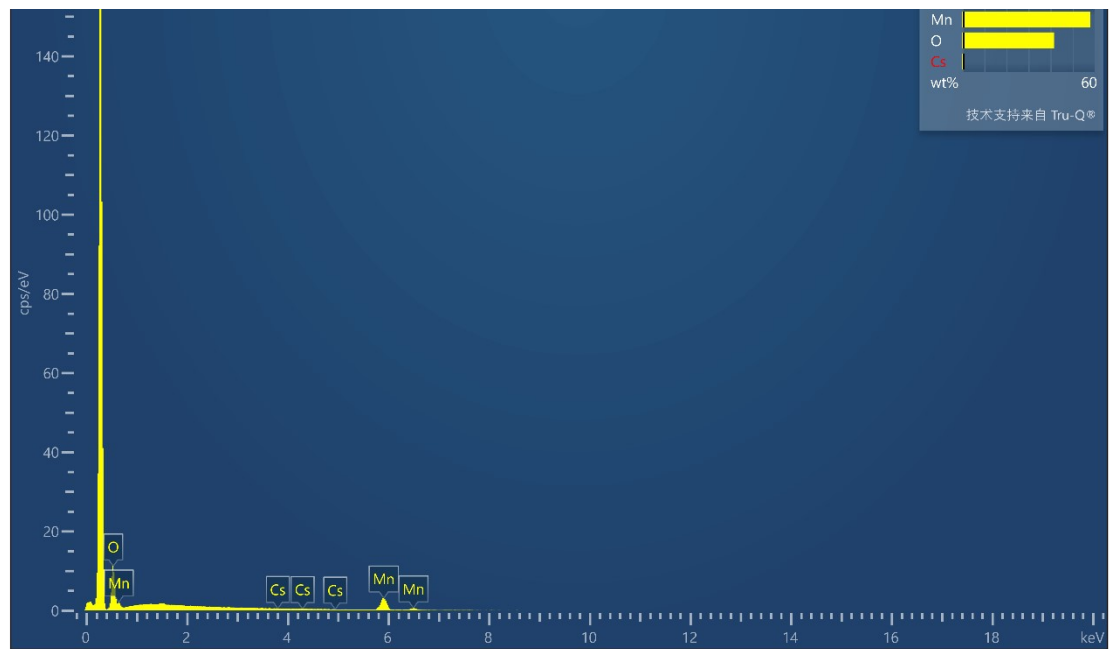


Fig. S5. EDS images of the CMO.

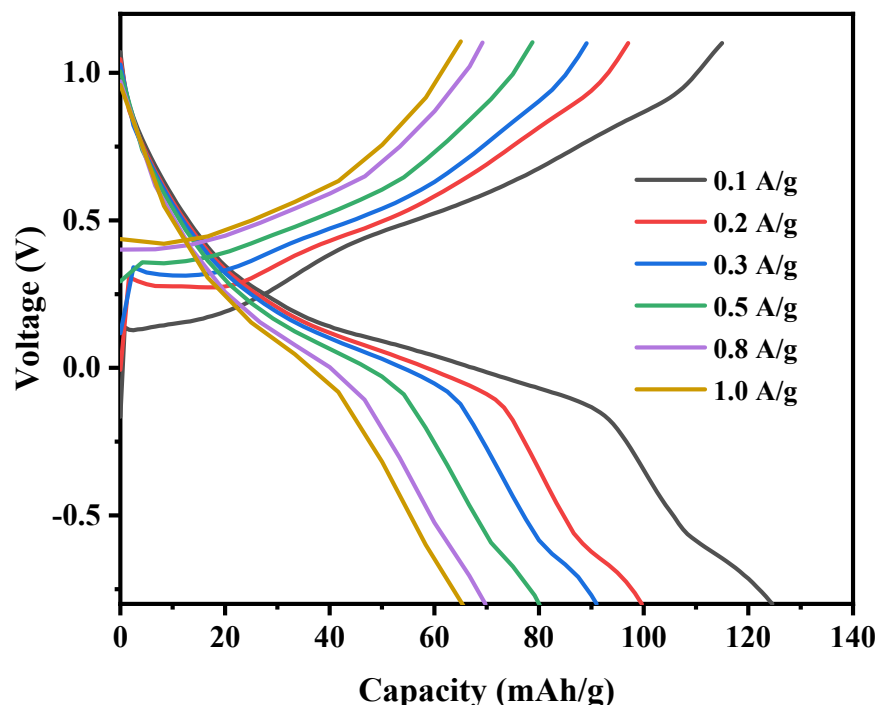


Fig. S6. GCD curves of the Mn_2O_3 at 0.1 A/g, 0.2 A/g, 0.3 A/g, 0.5 A/g, 0.8 A/g and 1.0 A/g.

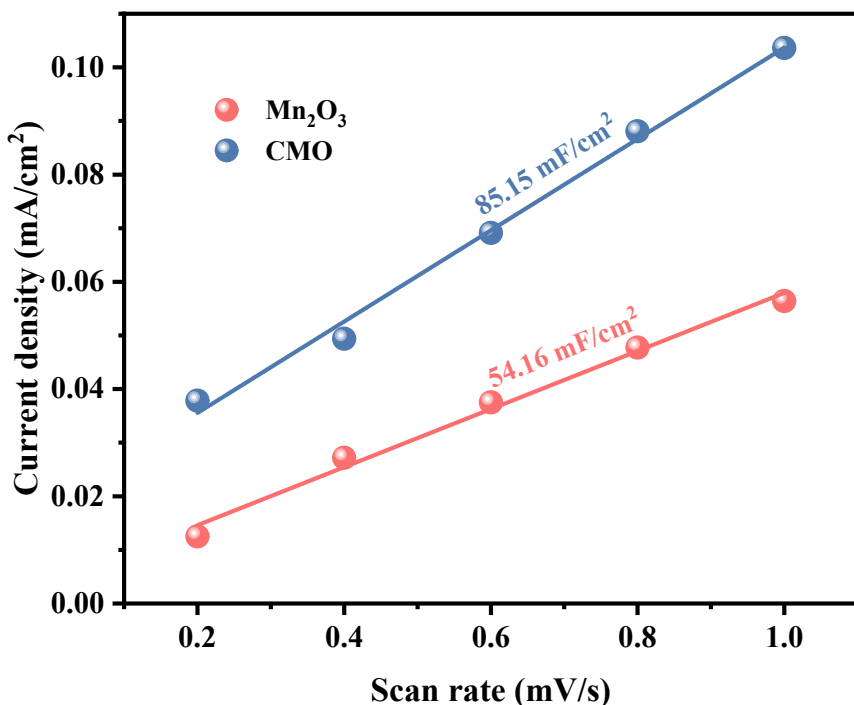


Fig. S7. The relationship between current density and scan rate of Mn_2O_3 and CMO.

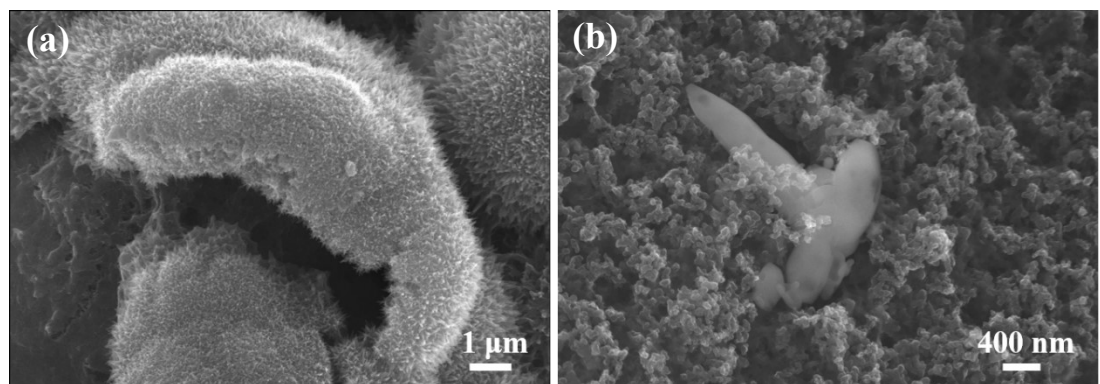


Fig. S8. (a) SEM images of Mn₂O₃ after 900 cycles. (b) SEM images of CMO after 1500 cycles.

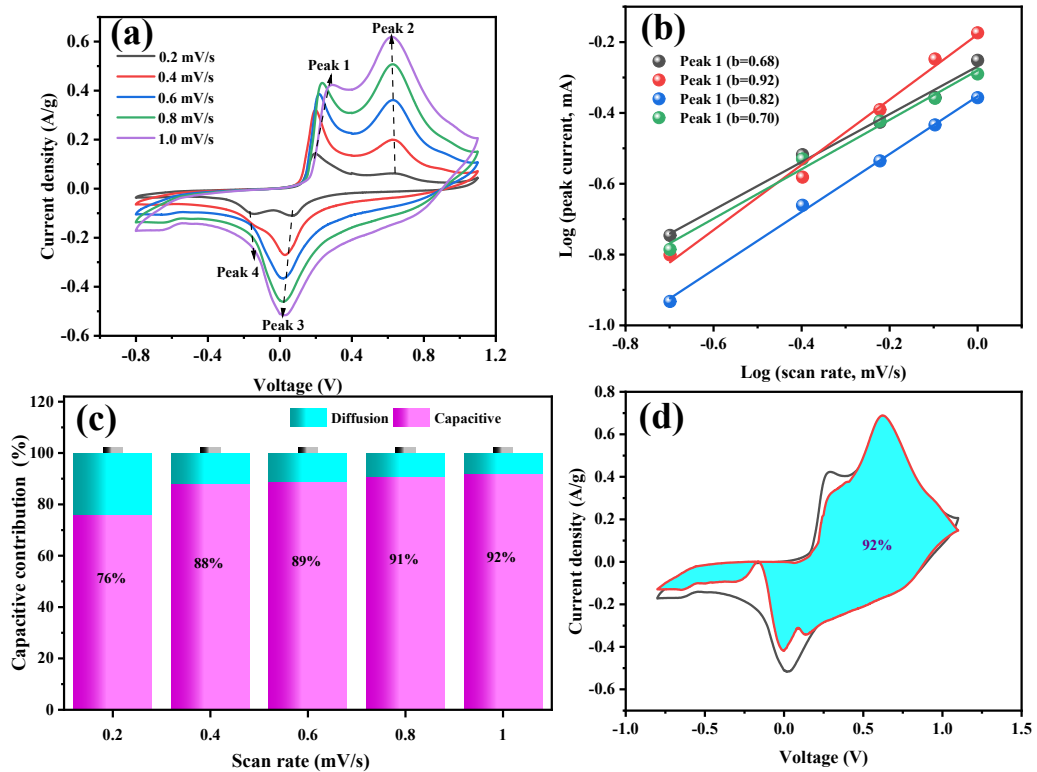


Fig. S9. (a) The CV curves of the Mn_2O_3 electrode at scan rates of 0.2, 0.4, 0.6, 0.8 and 1.0 mV/s. (b) The $\log (i)$ versus $\log (v)$ plots of corresponding four redox peaks in the CV curves of the Mn_2O_3 electrode. (c) The capacitive contributions at scan rates of 0.2, 0.4, 0.6, 0.8 and 1.0 mV/s of the Mn_2O_3 electrode in the 0.5 M MgSO_4 electrolyte. (d) The proportion of capacitance contribution of total capacity of the Mn_2O_3 electrode at a scan rate of 1.0 mV/s.

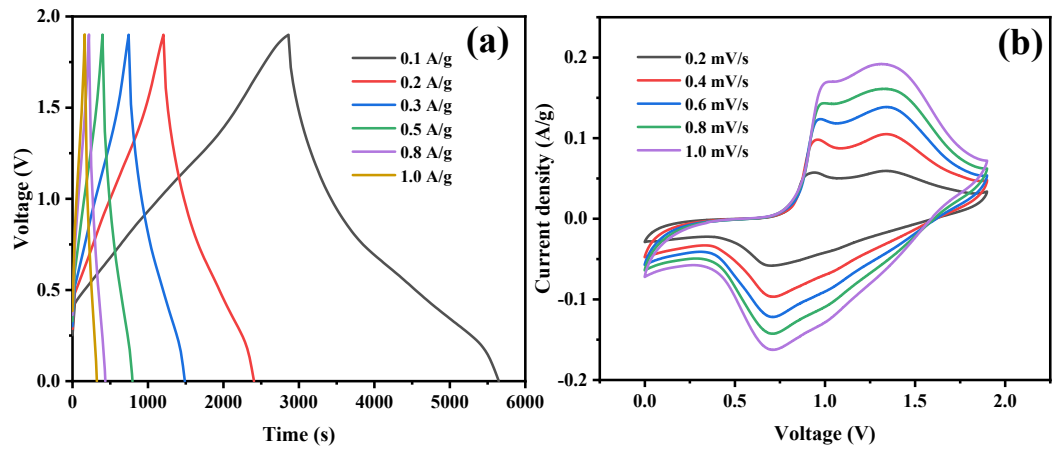


Fig. S10. (a) GCD curves of $\text{Mn}_2\text{O}_3/\text{AC}$ at 0.1 A/g, 0.2 A/g, 0.3 A/g, 0.5 A/g, 0.8 A/g and 1.0 A/g. (b) CV curves of $\text{Mn}_2\text{O}_3/\text{AC}$ at scan rate from 0.2 mV/s to 1.0 mV/s.

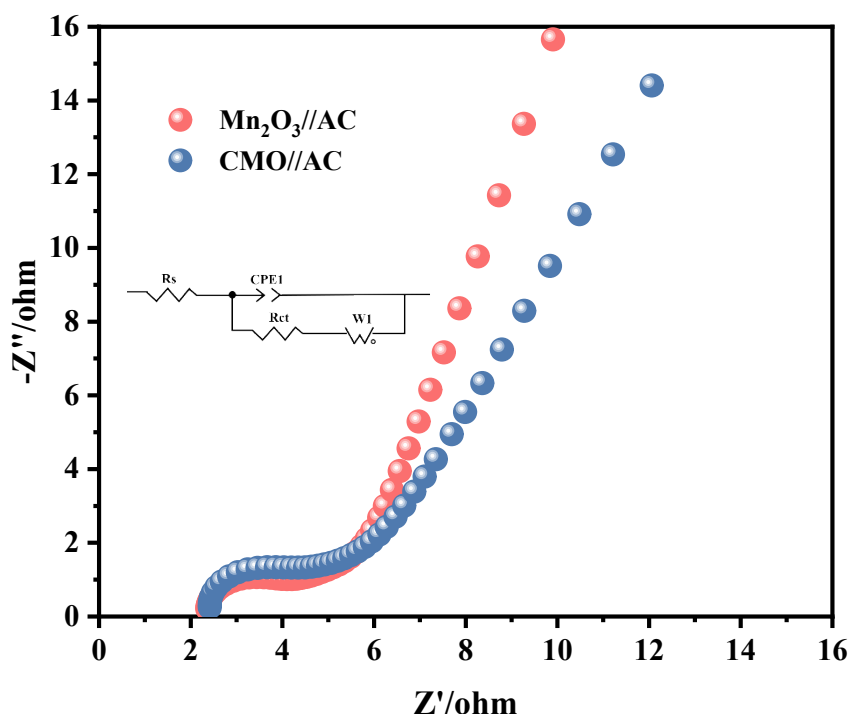


Fig. S11. Comparison of Nyquist plots of $\text{Mn}_2\text{O}_3/\text{AC}$ and CMO/AC at open-circuit voltage (the equivalent circuit diagram inset in the Figureure S8).



Fig. S12. Images of successful applications in (a) a watch and (b) a mobile phone.

Reference

1. Y. Ding, S. Zhang, J. Li, Y. Sun, B. Yin, H. Li, Y. Ma, Z. Wang, H. Ge, D. Su, T. Ma, *Adv. Funct. Mater.*, **2023**, 33, 2210519.
2. H. Zhang, D. Cao, X. Bai, *Inorg. Chem. Front.*, **2020**, 7, 2168-2177.
3. H. Zhang, K. Ye, K. Zhu, R. Cang, J. Yan, K. Cheng, G. Wang, D. Cao, *Chem. Eur. J.*, **2017**, 23, 17118-17126.
4. H. Zhang, D. Cao, X. Bai, H. Xie, X. Liu, X. Jiang, H. Lin, H. He, *ACS Sustainable Chem. Eng.*, **2019**, 7, 6113-6121.
5. H. Zhang, K. Ye, R. Cang, K. Zhu, J. Yan, K. Cheng, G. Wang, D. Cao, *J. Electroanal. Chem.*, **2017**, 807, 37-44.
6. H. Zhang, K. Ye, S. Shao, X. Wang, K. Cheng, X. Xiao, G. Wang, D. Cao, *Electrochim. Acta*, **2017**, 229, 371-379.
7. H. Zhang, K. Ye, K. Zhu, R. Cang, X. Wang, G. Wang, D. Cao, *ACS Sustainable Chem. Eng.*, **2017**, 5, 6727-6735.
8. H. Zhang, K. Ye, X. Huang, X. Wang, K. Cheng, X. Xiao, G. Wang, D. Cao, *J. Power Sources*, **2017**, 338, 136-144.
9. L. Chen, J. Bao, X. Dong, D. Truhlar, Y. Wang, C. Wang, Y. Xia, *ACS Energy Lett.*, **2017**, 2, 1115-1121.
10. F. Wang, X. Fan, T. Gao, W. Sun, Z. Ma, C. Yang, F. Han, K. Xu, C. Wang, *ACS Cent. Sci.*, **2017**, 3, 1121-1128.
11. X. Cao, L. Wang, J. Chen, J. Zheng, *ChemElectroChem*, **2018**, 5, 2789-2794.
12. Z. Pan, T. Qin, W. Zhang, X. Chu, T. Dong, N. Yue, Z. Wang, W. Zheng, *J. Energy*

Chem., **2022**, *68*, 42-48.

13. T. Sun, H. Du, S. Zheng, Z. Tao, *J. Power Sources*, **2021**, *515*, 230643.
14. T. Sun, X. Yao, Y. Luo, M. Fang, M. Shui, J. Shu, Y. Ren, *Ionics*, **2019**, *25*, 4805-4815.
15. C. Li, W. Wu, Y. Liu, X. Yang, Z. Qin, Z. Jia, X. Sun, *J. Power Sources*, **2022**, *520*, 230853.
16. H. Zhang, K. Ye, K. Zhu, R. Cang, J. Yan, K. Cheng, G. Wang, D. Cao, *Electrochim. Acta*, **2017**, *256*, 357-364.
17. D. Zhang, W. Huang, T. Chen, Q. Wang, T. Sun, *ACS Appl. Energy Mater.* **2021**, *4*, 6853-6865.
18. Y. Zhang, G. Liu, C. Zhang, Q. Chi, T. Zhang, Y. Feng, K. Zhu, Y. Zhang, Q. Chen, D. Cao, *Chem. Eng. J.*, **2020**, *392*, 123652.
19. D. Zhang, Y. Ma, J. Zhang, T. Sun, *Nanotechnol.*, **2021**, *32*, 44.
20. Q. Fu, X. Wu, X. Luo, S. Indris, A. Sarapulova, M. Bauer, Z. Wang, M. Knapp, H. Ehrenberg, Y. Wei, S. Dsoke, *Adv. Funct. Mater.*, **2022**, *32*, 2110674
21. Z. Shi, L. Xue, J. Wu, Q. Guo, Q. Xia, M. Ni, P. Wang, S. Savilov, S. Aldoshin, F. Zan, H. Xia, *J. Electrochem. Soc.*, **2021**, *168*, 120549.
22. W. Wang, Y. Fang, S. Wang, Z. Zhang, R. Zhao, W. Xue, *J. Alloy. Compd.*, **2022**, *900*, 163532.
23. Y. Zhu, M. Chen, M. Dong, Q. Zhang, W. Ma, M. Zeng, S. Zou, L. Sheng, Z. Yang, *Energy Fuels*, **2022**, *36*, 7829-7840.
24. Z. Liu, G. Pang, S. Dong, Y. Zhang, C. Mi, X. Zhang, *Electrochim. Acta*, **2019**, *311*,

1-7.

25. M. Liang, X. Li, Y. Kang, N. RehmanLashari, X. Zhang, Y. Zhao, H. Wang, Z. Miao, C. Fu, *J. Power Sources*, **2022**, *535*, 231486.
26. S. Jiang, Y. Qiao, T. Fu, W. Peng, T. Yu, B. Yang, R. Xia, M. Gao, *ACS Appl. Mater. Interfaces*, **2021**, *13*, 34374-34384.
27. Z. Hou, X. Li, J. Liang, Y. Zhu, Y. Qian, *J. Mater. Chem. A* **2015**, *3*, 1400-1404.
28. A. Elgendi, N. Basiony, F. Heakal, A. Elkholy, *J. Power Sources*, **2020**, *466*, 228294.
29. M. Shi, M. Zhao, L. Jiao, Z. Su, M. Li, X. Song, *J. Power Sources*, **2021**, *509*, 230333.
30. S. Zhang, H. Chen, Y. Xu, C. An, K. Xiang, *Rare Met.*, **2022**, *41*, 3129-3141.